Eur. Phys. J. A **20**, 119–122 (2004)
DOI 10.1140/epja/i2002-10336-9

THE EUROPEAN PHYSICAL JOURNAL A

Spherical shell model description of deformation and superdeformation

A. Poves[1,a], E. Caurier[2], F. Nowacki[2], and A. Zuker[2]

[1] Departamento de Física Teórica, Universidad Autónoma de Madrid, Cantoblanco, 28049 Madrid, Spain
[2] Institut de Recherches Subatomiques, IN2P3-CNRS-Université Louis Pasteur, F-67037 Strasbourg Cedex 2, France

Received: 29 October 2002 /
Published online: 16 March 2004 –

Abstract. Large-scale shell model calculations give at present a very accurate and comprehensive description of light and medium-light nuclei, specially when $0\hbar\omega$ spaces are adequate. The full pf-shell calculations have made it possible to describe many collective features in an spherical shell model context. Calculations including two major oscillator shells have proven able to describe also superdeformed bands.

PACS. 21.60.Cs Shell model – 21.60.-n Nuclear structure models and methods – 21.10.Hw Spin, parity, and isobaric spin – 21.10.Ky Electromagnetic moments

1 Introduction

The spherical shell model approach to the nuclear dynamics has three main ingredients: the effective interaction, the valence space and the computational tools that make it possible to solve the huge secular problems involved. Our understanding of the effective interaction used in shell model calculations changed radically through the realization of the key spectroscopic role played by the monopole terms of the Hamiltonian that determine the evolution of the spherical single-particle orbits and the relative location of the different configurations [1], setting the initial conditions for the action of the correlation terms of the nuclear force (pairing, quadrupole, etc.). A new generation of shell model codes, that can treat problems involving basis dimensions as large as a few billions, has opened the possibility to access new regions of the chart of nuclides [2]. Full $0\hbar\omega$ calculations in the pf-shell have demonstrated the ability of the spherical shell model to treat in an unified framework all the variety of nuclear excitations: single-particle modes, neutron-neutron and proton-neutron pairing correlations, rotational bands based upon well-deformed intrinsic states, etc. [3]. Other collective manifestations such as backbending, alignment, superfluid moments of inertia, etc., until now confined to the realm of heavy nuclei and treated by deformed mean-field models, have been experimentally found in medium-light nuclei using the large γ-detectors GASP, EUROBALL and GAMMASPHERE [4,5]. The shell model calculations have predicted or explained this full panoply of effects. More recently, excited superdeformed bands have been experimentally found in ^{36}Ar and ^{40}Ca [6,7]. As we shall discuss in this paper, shell model configurations involving 4p-4h and 8p-8h excitations from the *sd*- to the pf-shell account nicely for its more salient features [8].

[a] e-mail: alfredo.poves@uam.es

2 Superdeformed bands in ^{36}Ar and ^{40}Ca

The existence of excited deformed bands in spherical nuclei is a well documented fact, dating back to the '60s. A classical example is provided by the four-particle–four-holes (4p-4h) and eight-particles–eight-holes (8p-8h) states in ^{16}O, starting at 6.05 MeV and 16.75 MeV of excitation energy [9,10]. However, it is only recently that similar bands, of deformed and even superdeformed character, have been discovered in other medium-light nuclei such as ^{56}Ni [5], ^{36}Ar [6] and ^{40}Ca [7] and explored up to high spin. One characteristic feature of these bands is that they belong to rather well-defined spherical shell model configurations. For example, the deformed excited band in ^{56}Ni can be associated with the configuration $(1f_{7/2})^{12}$ $(2p_{3/2}, 1f_{5/2}, 2p_{1/2})^4$ while the (super)deformed band in ^{36}Ar has the structure $(sd)^{16}$ $(pf)^4$. The states we aim to are dominantly core excitations from the *sd*-shell to the pf-shell. The natural valence space would thus comprise both major oscillator shells. However, the inclusion of the $1d_{5/2}$ orbit in the valence space produces a huge increase in the size of the basis and massive center-of-mass effects, thus we are forced to exclude it from the valence space; this is equivalent to take a closed core of ^{28}Si. We are aware that this truncation will reduce slightly the quadrupole coherence of the solutions. Our valence space will consist of the

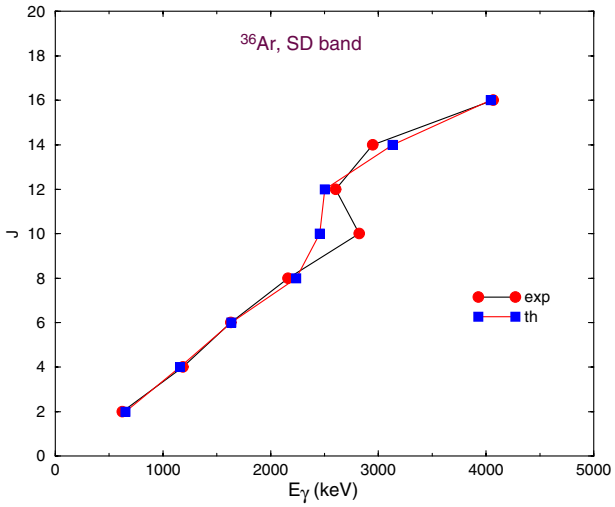

Fig. 1. The superdeformed band in ^{36}Ar: experimental *vs.* 4p-4h calculation.

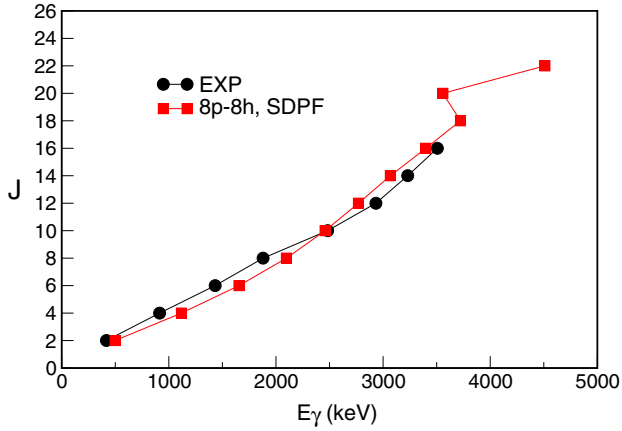

Fig. 2. The superdeformed band in ^{40}Ca: experimental *vs.* 8p-8h calculation.

Table 1. Quadrupole properties of the 4p-4h configuration yrast band in ^{36}Ar (in e^2 fm^4 and e fm^2).

	$B(E2)(J \to J-2)$				
J	EXP	TH	$Q_{\rm spec}$	$Q_0(s)$	$Q_0(t)$
2		315	−36.0	126	126
4	372(59)	435	−45.9	126	124
6	454(67)	453	−50.7	127	120
8	440(70)	429	−52.8	125	114
10	316(72)	366	−52.7	121	104
12	275(72)	315	−53.0	119	96
14	232(53)	235	−54.3	120	82
16	> 84	131	−56.0	122	61

orbits $2s_{1/2}$, $1d_{3/2}$, $1f_{7/2}$, $2p_{3/2}$, $1f_{5/2}$, $2p_{1/2}$. The effective interaction is the same used in ref. [6] denoted *sdpf.sm*.

In the ^{36}Ar case we proceed to solve the secular problem in the 4p-4h space. In fig. 1 the calculated energy levels are compared with the experimental results in a backbending plot. The agreement is excellent, except at $J = 12$ where the data show a clear backbending while the calculation produces a much smoother upbending pattern. In the experimental data there is a close-by second 10^+ state, therefore, the discrepancy may be due to the lack of mixing in the calculation.

In table 1 we have collected the quadrupole properties of the superdeformed band. We have computed the $B(E2)$'s and the spectroscopic quadrupole moments $Q_{\rm spec}$ using standard effective charges $\delta q_\pi = \delta q_\nu = 0.5$. The intrinsic (transition) quadrupole moments $Q_0(t)$ are extracted from the $B(E2)$'s and the static ones $Q_0(s)$ from the spectroscopic quadrupole moments. We assume $K = 0$ and use the standard formulas relating laboratory and intrinsic frame quantities. Both $Q_0(s)$ and $Q_0(t)$ are nearly equal and reasonably constant up to the backbending region where they diverge indicating the onset of the alignment regime. The comparison with the experimental $B(E2)$'s from ref. [11] is remarkably good. Actually, it can be seen to be better than it was in [11]. The reason is that the theoretical numbers in ref. [11] were inadvertently computed with the default value of the oscillator size parameter in our codes, $b = 1.01\ A^{1/6}$ fm, which is 5% smaller than the correct one for these light nuclei. The value of the intrinsic quadrupole moment corresponds roughly to a deformation $\beta = 0.5$, so we can speak of a nearly superdeformed band up to $J = 10$–12.

We move now to the study of the superdeformed band of ^{40}Ca, recently measured at GAMMASPHERE [7]. When we analyse the maximum quadrupole content of the different np-nh spaces in ^{40}Ca, either in the $SU(3)$ limit or reasoning in terms of Nilsson diagrams, we conclude that the only possible candidate to produce a superdeformed band is the 8p-8h space. This surmise is borne out by the calculations and therefore we shall refer from now on to the 8p-8h results. In ^{40}Ca, the valence space adopted for ^{36}Ar leads to very large basis dimensions (2×10^9 for the complete calculation of 12 particles). The dimension of the 8p-8h space is still very large (4.5×10^8) therefore we have to draw in our experience in the pf-shell, to reduce still a bit the dimensions (to 2.2×10^8) by limiting the maximum number of particles in the $1f_{5/2}$ and $2p_{1/2}$ orbits to two, a truncation that produces results that are already very close to the complete ones.

The gamma-ray energies along the yrast sequence are compared to the experimental results (Band 1 in ref. [7]) in fig. 2 in the form of a backbending plot. The calculation reproduces very satisfactorily the experimental results. The only difference is the change of slope in the experimental curve at $J = 10$, not reproduced by the calculation; this is probably due to local mixing. Notice that the experimental band is very regular, showing no backbending up to the highest measured spin, $J = 16$, contrary to the situation in ^{48}Cr [4] where the backbending takes place at $J = 12$. The calculated band is also very regular and backbends only at $J = 20$ which is the band termination for the configuration $(1f_{7/2})^8\ (1d_{3/2}\ 2s_{1/2})^{-8}$. The yrast state with $J = 22$ corresponds to configurations of the type $(1f_{7/2})^7\ 2p_{3/2}\ (1d_{3/2}\ 2s_{1/2})^{-8}$ and beyond. The delay in the alignment

Table 2. Quadrupole properties of the 8p-8h configuration's yrast band in ^{40}Ca, calculated in the *sdpf* valence space.

J	$B(E2)(J \to J-2)$	$Q_{\rm spec}$	$Q_0(t)$	$Q_0(s)$
2	589	−49.3	172	172
4	819	−62.4	170	172
6	869	−68.2	167	171
8	860	−70.9	162	168
10	823	−71.6	157	164
12	760	−71.3	160	160
14	677	−71.1	149	157
16	572	−72.2	128	158
18	432	−75.0	111	162
20	72	−85.1		
22	8	−79.1		
24	7	−81.5		

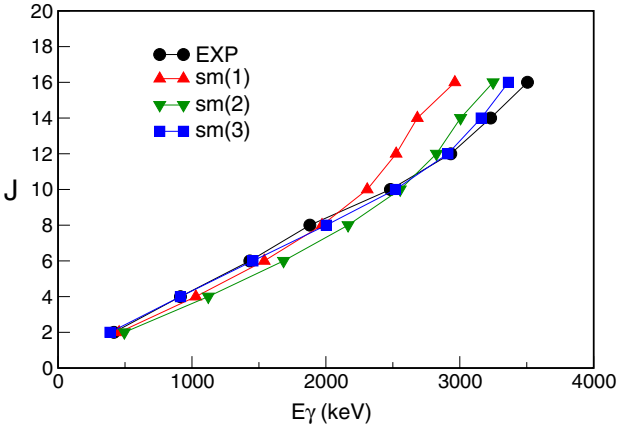

Fig. 3. The superdeformed band in ^{40}Ca: experimental *vs.* different 8p-8h calculations in the *zbm*2 valence space.

is surely due to the extra collectivity induced by the presence of *sd* particles in Pseudo-$SU(3)$ orbitals.

In table 2 we have collected the quadrupole properties of the superdeformed band. We have computed the $B(E2)$'s and the spectroscopic quadrupole moments $Q_{\rm spec}$ as in the ^{36}Ar case. As expected, both $Q_0(s)$ and $Q_0(t)$ are very large, nearly equal and reasonably constant up to the band termination, a fact that supports the existence of a robust intrinsic state. The calculated Q_0 value of 172 e fm^2 is in very good agreement with the experimental value $Q_0(t) = 1.80^{+0.39}_{-0.29}$ e b, obtained from the fractional Doppler shifts. This experimental value corresponds to a deformation $\beta \sim 0.6$, *i.e.* to a superdeformed shape. The calculation predicts a slight decrease of the deformation with increasing J, while experimentally it seems to remain constant until the highest measured spin state ($J = 16$). This departure may be due to the blocking of the $1d_{5/2}$ orbital. Despite that, the calculation at fix particle-hole number contains most of the relevant physics of the superdeformed band in ^{40}Ca. The deformation that our calculation produces is probably the highest ever obtained in a shell model calculation describing a "bona fide" rotational band. As a matter of fact it almost saturates the $SU(3)$ limit of the intrinsic quadrupole moment in these two major shells ($Q_0 = 226$ e fm^2), or the —more realistic— quasi-$SU(3)$ one ($Q_0 = 180$ e fm^2). At the band termination, the $B(E2)$'s drop to zero while the spectroscopic quadrupole moments keep constant, reflecting the transition from the collective to the aligned regime. In ^{36}Ar the $SU(3)$ and quasi-$SU(3)$ limits are $Q_0 = 173$ e fm^2 and $Q_0 = 136$ e fm^2, respectively. The calculated value, $Q_0 = 126$ e fm^2 is also very close to the quasi-$SU(3)$ prediction.

The next step is the study of the mixing of the different np-nh configurations. Unluckily, in this valence space, this goal is definitely beyond our computational possibilities —even with the truncation adopted above— because it demands the calculation of many states of the same total angular momentum. We try to circumvent these limitations by reducing once more the valence space, eliminating completely the upper pf-shell orbits. The active orbits will then be $2s_{1/2}$, $1d_{3/2}$, $1f_{7/2}$, $2p_{3/2}$. This valence space will be called *zbm*2, to emphasize its links with the space ($1p_{1/2}$, $1d_{5/2}$, $2s_{1/2}$) used in the late '60s to describe the core excited states of ^{16}O [12]. We have tried to evaluate the effects of this further truncation by comparing the 8p-8h results in the two spaces, with the interaction *sdpf.sm*. The the new γ-energies are presented in fig. 3 under the label *sm*(1).

The yrast band behaves nicely for the lower spins, but is too compressed beyond $J = 10$. The quadrupole collectivity turns out to be a 10% smaller and decreases more rapidly at high spins than it does in the fuller calculation. This suggests that an increase of the quadrupole-quadrupole interaction in the pf sector of the interaction could mock the full space results. Therefore, we have increased a 10% the qq interaction and repeated the calculations in the *zbm*2 space. The results for the energies are plotted in fig. 3 (label *sm*(2)), and we see that the band has now a much better behaviour and the correct span. However, the quadrupole properties remain basically unchanged. We have tried other interactions and/or renormalizations and our conclusion is that any decent interaction produces the same intrinsic state, *i.e.* the quadrupole collectivity has reached saturation in this valence space. In order to increase the deformation and to keep it constant for the higher spins one must enlarge the valence space, this will increase the intrinsic quadrupole moment a 10% upon inclusion of the upper pf-shell and another 10% upon opening the $1d_{5/2}$ orbital. Thus, if we keep the usual effective charges, we have to be aware that the quadrupole coherence in the *zbm*2 space will always be a 20% smaller than in the full space of the two major shells.

A new interaction has been built recently, specifically for the *zbm*2 valence space, and used to describe the radii isotope shifts in the Calcium isotopes [13]. It was based on *sdpf.sm* with mostly monopole changes. Following our discussion above, we have increased a ten percent the quadrupole-quadrupole interaction in the pf sector of the *zbm*2 space. In addition, in [13] an off-diagonal, cross-shell schematic isovector pairing was subtracted from the initial interaction to avoid double counting. Here, we choose to reduce all the off-diagonal cross-shell matrix elements

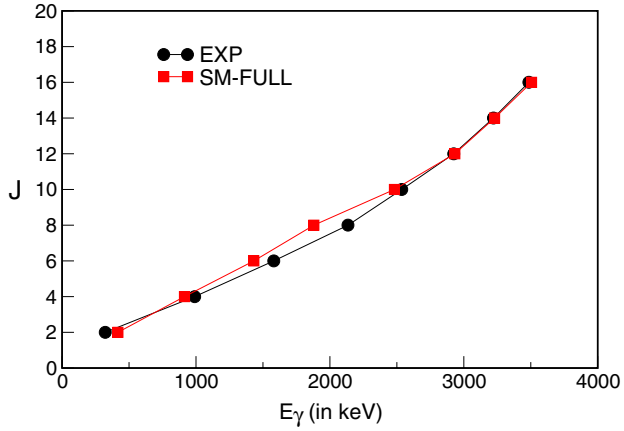

Fig. 4. The superdeformed band in ^{40}Ca: experimental *vs.* full calculation in the *zbm*2 valence space.

a 25%. It is with this interaction that we shall proceed to study the mixing. The results for the fixed 8p-8h configuration can be found also in fig. 3 with the label $sm(3)$. As expected both the energies and the quadrupole properties are very close to the $sm(2)$ set.

The final step consists in finding the mixing among the different np-nh configurations. This is a formidable task because the np-nh series is not easy to truncate. In earlier studies [14] we have reached the conclusion that, in order to have the correct mixing in a given np-nh configuration, the valence space must contain at least all the configurations up to (np + 4)-(nh + 4). This is easy to understand, because the pairing interaction mixes configurations that are 2p-2h apart. But the amount of mixing depends also of their relative position, therefore, if the configurations that are 4p-4h apart are not included, the 2p-2h ones will be too high and will not renormalize the reference states properly. That is why the *zbm*2 valence space cannot provide the proper renormalization to the 8p-8h band, because the 10p-10h and 12p-12h configurations cannot develop enough collectivity due to the closure of the $1d_{5/2}$ orbit. This has two effects: first, as these configurations lay much too high in energy, they do not mix enough with the 8p-8h ones and the reduced gain in energy has to be compensated with an artificial lowering of the 8p-8h configurations. But even doing that, the absence of mixing with other configurations that have similar of larger quadrupole contents, makes the mixed results unphysically less collective than the unmixed ones. With all these caveats we have tried to get a first glimpse on the mixed results, that we comment now briefly. We have played freely with the *sd-pf* global monopoles in order to locate the three lower 0^+ states of ^{40}Ca close to their experimental values. The structure of the ground state is the expected one, about 60% closed shell, with mainly 2p-2h mixing. The first excited 0^+ is dominantly (60%) 4p-4h with mainly 6p-6h and 8p-8h mixing. It corresponds to the bandhead of the experimental Band 2. The third one is 60% 8p-8h, and the mixing is dominantly 4p-4h. The 10p-10h and 12p-12h component are —as we had anticipated— completely absent. The calculation of the three lower 0^+ is straightforward, however, the calculation of the excited states belonging to the 4p-4h or the 8p-8h bands is not, because these are most often drowned in a sea of other uninteresting states. To overcome this difficulty we select as starting vectors in the Lanczos procedure the eigenstates of the band obtained in the np-nh space. This choice accelerates the convergence of the states we are seeking and makes it possible to keep track of them in case of fragmentation. We have used this method to obtain the mixed superdeformed band, starting with the 8p-8h states. The excitation energies change little, but enough to improve the quality of the agreement with the experimental data of the 8p-8h calculation (see fig. 4). However, the quadrupole moments and transition probabilities get eroded —30% to 50%— by the mixing or even completely washed out at the top of the band. As we have discussed above, this is an intrinsic limitation of the valence space that we cannot overcome for the moment.

In conclusion, we have performed a study of the many-particle–many-hole configurations in ^{36}Ar and ^{40}Ca, aiming to understand its recently discovered superdeformed excited bands. We have shown that the yrast bands of the 4p-4h and 8p-8h configurations in the *sd-pf* valence space reproduce very well the experimental results and represent a textbook example of the description of superdeformed bands in the framework of the spherical shell model.

This work is supported by the Spanish Ministry of Science and Technology under grant BFM2000-30 and by the IN2P3(France)-CICyT(Spain) Collaboration.

References

1. M. Dufour, A.P. Zuker, Phys. Rev. C **54**, 1641 (1996).
2. E. Caurier, ANTOINE code, Strasbourg (1989-2002...); E. Caurier, F. Nowacki, Nathan code Strasbourg (1995-2002...).
3. E. Caurier *et al.*, Phys. Rev. C **59**, 2033 (1999).
4. S.M. Lenzi *et al.*, Z. Phys. A **354**, 117 (1996).
5. D. Rudolph *et al.*, Phys. Rev. Lett. **82**, 3763 (1999).
6. C.E. Svensson *et al.*, Phys. Rev. Lett. **85**, 2693 (2000).
7. E. Ideguchi *et al.*, Phys. Rev. Lett. **87**, 222501 (2001).
8. E. Caurier *et al.*, arXiv nucl-th/0205036.
9. E.B. Carter, G.E. Mitchell, R.H. Davis, Phys. Rev. **133** 1421 (1964).
10. P. Chevallier, F. Scheibling, G. Goldring, I. Plesser, M.W. Sachs, Phys. Rev. **160**, 827 (1967).
11. C.E. Svensson *et al.*, Phys. Rev. C **85**, 061301 (2000).
12. A.P. Zuker, B. Buck, J.B. McGrory, Phys. Rev. Lett. **21**, 39 (1968).
13. E. Caurier *et al.*, Phys. Lett. B **87**, 240 (2001).
14. A. Poves, J. Sánchez Solano, E. Caurier, F. Nowacki, arXiv nucl-th/0210069.